Multiple contact compression tests on sand particles

Todisco, M. C.; Wang, W.; Coop, M. R.; Senetakis, K.

Published in:
Soils and Foundations

Published: 01/02/2017

Document Version:
Final Published version, also known as Publisher's PDF, Publisher's Final version or Version of Record

Published version (DOI):
10.1016/j.sandf.2017.01.009

Publication details:
Todisco, M. C., Wang, W., Coop, M. R., & Senetakis, K. (2017). Multiple contact compression tests on sand particles. *Soils and Foundations*, *57*(1), 126-140. https://doi.org/10.1016/j.sandf.2017.01.009

HOSTED BY
ELSEVIER
CrossMark
Available online at www.sciencedirect.com
ScienceDirect
Soils and Foundations 57 (2017) 126–140
SOILS AND FOUNDATIONS
www.elsevier.com/locate/sandf

Multiple contact compression tests on sand particles ☆

M.C. Todisco [a], W. Wang [a,*], M.R. Coop [b,1], K. Senetakis [a]

[a] City University of Hong Kong, Hong Kong
[b] University College London, United Kingdom

Received 25 April 2016; received in revised form 11 October 2016; accepted 3 November 2016
Available online 8 February 2017

Abstract

Particle crushing has been recognised as being of key importance for many engineering applications. In soil mechanics, this phenomenon has become crucial for defining a complete framework capable of describing the mechanical behaviour of sands. In this study, the effect of multiple discrete contacts on the breakage of grain particles was investigated by crushing coarse grains of a quartz sand and a crushed limestone sand between a number of support particles, thereby varying the number of contacts, i.e., the coordination number. The stress at failure was calculated when the particles broke, which occurred through a number of distinct modes, namely, chipping, splitting or fragmenting, which were observed with the use of a high-speed microscopic camera. The Weibull criterion was applied to calculate the probability of surviving grain crushing, and the fracture modes were observed for each configuration of supporting particles. The data showed that in addition to the number of contacts, the nature of those contacts, controlled by particle morphology and mineralogy, also plays a significant role in determining the strength of a particle. The sphericity affected the strength of the softer limestone sand, while the local roundness at the contacts was important for the harder quartz sand. Catastrophic explosive failure was more often observed in particles with harder contacts, while softer contacts tended to mould relative to their neighbouring particles inducing a more frequent ductile mode of crushing.

Keywords: Multi-particle compression tests; Micro-mechanics; Failure mode; Particle morphology

1. Introduction

Understanding particle crushing is very important for modelling, simulating, and optimising mineral and powder processing (Tavares, 2007). And, in soil mechanics, establishing a link between particle breakage phenomena and the macro-mechanical behaviour of sands has become of key importance (McDowell and Bolton, 1998; McDowell, 2002; Coop et al., 2004; Muir Wood, 2008; Altuhafi and Coop, 2011). Failure models accounting for the coordination number, CN, in an assembly of grains have been developed by many authors, for example Tsoungui et al. (1999) and Ben-Nun and Einav (2010) among others. In an assembly of poly-dispersed granular materials, the breaking process of the soil matrix depends on the strength of each grain, which varies with its size and the number of contacts established between grains, since the forces transferred within the assembly vary with the number of contact points. Contact force networks inside an assembly of discs have been determined through the use of photo-elasticity techniques (Drescher and De Jong, 1972; Durelli and Wu, 1984). However, it is difficult to define the stress evolution in a system of sand specimens since the photo-elasticity method cannot be applied to sand particles, although Fonseca et al. (2016) have inferred the strong

Peer review under responsibility of The Japanese Geotechnical Society.
☆ This manuscript was submitted to the Special Issue on the International Symposium on Geomechanics from Micro to Macro IS-Cambridge 2014 (Vol.56 No.5).
* Corresponding author.
E-mail address: wanyiwang2-c@my.cityu.edu.hk (W. Wang).
[1] Formerly City University of Hong Kong, Hong Kong.

http://dx.doi.org/10.1016/j.sandf.2017.01.009
0038-0806/

force network from an analysis of particle contacts with X-ray CT. Numerical simulations have explored the stress distributions which lead to the failure of an individual grain subjected to a system of forces within an assembly (Ben-Nun and Einav, 2010; Minh and Cheng, 2013). Gundepudi et al. (1997) extended the solution for the stress distribution in an elastic sphere under a single contact load (Dean et al., 1952) to spheres under multiple contacts. Numerically they found that the maximum stress away from the contact region was similar for uniaxial and four-point loading on different planes of the sphere, larger for three-point in-plane loading, and smaller for six contact points. However, they also observed experimentally that the failure of glass and aluminium spheres initiated in the proximity of the contacts, where the contact forces reached the maximum.

In rock engineering, the Brazilian test has been used to indirectly assess the tensile strength of brittle materials. Li and Wong (2013) reviewed the mechanism of crack initiation inside the disc of a rock. They found numerically that cracks in a disc subjected to two opposing forces might originate near the two loading points along the central axis when the tensile strain surpasses a certain critical tensile strain threshold, or at the centre of the contact when the tensile stress surpasses the critical tensile stress threshold. However, if a fracture initiates far from the centre of the disc, the Brazilian test is not appropriate for measuring the tensile strength of the rock (Fairhurst, 1964). For point load tests on an elastic sphere, Russell and Muir Wood (2009) gave an analytical solution showing that the initial failure would occur just below the contact point and that it was of the shearing type, the failure criterion being dependent on the second invariant of the stress tensor. Russell et al. (2009) applied the same failure criterion to particles subjected to multi-contact loading within several different regular packings of spheres. The failure initiated near the largest contact force, when the ratio of the second to the first invariant of the stress tensor was the largest of the localised maxima, independent of the material properties or the particle size. However, the yield or failure of the assembly would depend on both the maximum contact forces and the stability of the assembly.

Based on CT images, Zhao et al. (2015) were able to relate the internal features of quartz and decomposed granite particles to their geological origins and to explore how these features affected their mode of crushing. The single-particle crushing tests on quartz grains showed that the crushing occurred along tensile planes roughly parallel to the loading direction, although conchoidal in shape. However, they also observed an extensive fragmentation at the contact points, as also shown by Gundepudi et al. (1997), which might have been generated by shear failure, as described by Russell and Muir Wood (2009).

This experimental study is an extension of the preliminary results by Todisco et al. (2015) who performed multiple, but discrete, contact crushing tests on 60 particles of crushed limestone and 68 particles of a quartz sand from the UK. The updated testing programme comprises 362 and 233 tests on quartz and crushed limestone, respectively, the very large number of tests allowing for a much clearer assessment of the factors affecting the breakage. The data were interpreted in terms of nominal stresses, i.e., characteristic stresses, which might not accurately reproduce the real stress distributions within the particles under compressive loads, but they offer the basis for a statistical comparison between the different types of compressive loading. Specimens were tested by varying the number of contact forces on the particles, i.e., the coordination number, CN. The stress at failure was calculated when the particle broke, which was through a number of distinct modes, namely, chipping, splitting or fragmenting. The Weibull criterion (Weibull, 1951) was applied to calculate the probability of surviving grain crushing, and the influences of particle morphology and mineralogy on failure were investigated.

2. Materials, equipment, and testing procedures

The crushing tests were performed at a constant rate of 0.1 mm/min in a modified CBR apparatus equipped with a high-speed camera with a microscopic lens of maximum magnification of 16× (Fig. 1). The fastest frame rate of the camera was 2130 frames/s; however, tests were conducted at 1000 frames/s because this gave the best compromise between capturing time and exposure, and thus, the best picture quality (Wang and Coop, 2016). The forces and displacements were measured with a load cell with a capacity of 1000 N, a resolution of 0.1 N, and an LVDT with a linear range of ±3.5 mm and a resolution of 1 μm. The crushed particle, No. 1 in Fig. 2, was placed between others, which in turn were glued onto steel mounts using epoxy resin. The mounts were fixed into brass wells. The lower of the two was fixed to an aluminium platen which,

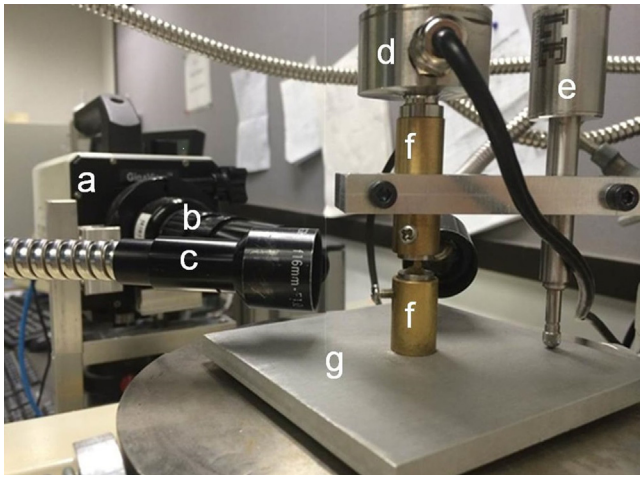

Fig. 1. Equipment for multi-axial crushing tests: (a) high speed camera; (b) microscope lens; (c) additional lighting system with focussing lenses; (d) load cell; (e) LVDT; (f) brass wells containing steel mounts; and (g) base support resting on ball bearings.

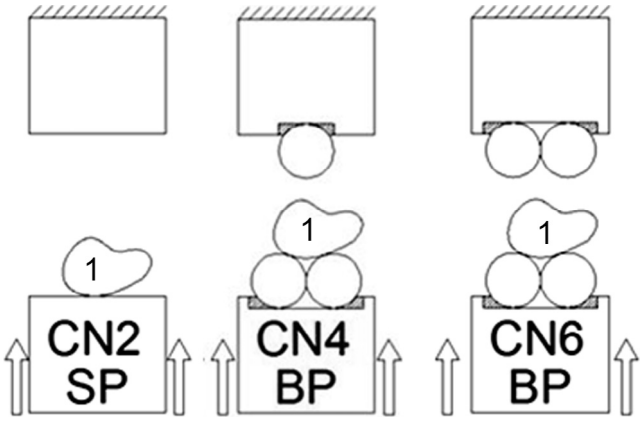

Fig. 2. Schematic representation of multi-contact crushing tests for particles tested between hardened steel mounts (SP), between 4 steel balls (CN4-BP), and between 6 steel balls (CN6-BP).

in turn, was placed onto ball bearings in order to release the lateral restraint and to ensure that the exact number of loading contacts occurred between the crushed particle and the others.

Wang and Coop (2016) also investigated single particle crushing with high-speed photography, but the aim of their work was to investigate the effects of the number and the nature of the contacts. This photographic technique allows much larger numbers of particles to be tested than CT scanning, so that strength distributions may be determined. The tests were performed in three different configurations, varying the number of contacts, CN, between the crushed particle and the others. The three different modes of the tests are described in Fig. 2. When the particle is crushed between two hardened steel mounts, the test is the standard single-particle crushing test (Nakata et al., 1999); when the particle is crushed between three particles at the bottom and one at the top, the test is a multi-particle crushing test with a CN equal to 4; and when there are three particles at both the bottom and the top, the test is the multi-particle crushing test with a CN equal to 6. It is emphasised that in the SP test, an irregular sand particle has at least three points of contact if it is at rest on a horizontal plane and four points if it is crushed between flat surfaces. However, the configurations for the SP and CN4 in this paper are likely to be different because the contacts of the former would be in closer proximity. The single-particle crushing tests have therefore been identified as SP. The differences in strength between the two types of tests will be discussed below. The test configurations used here are the only ones available for which the number of contacts can be ensured. While Russell et al. (2009) was able to numerically investigate the behaviour of particles within regular arrays of perfectly equal-sized spheres, these packings cannot be used in experimental work on real particles.

The coordination number, CN, and the type of support particles (steel balls, BP, or sand particles, PP) define the type of test. For example, CN4-BP refers to a test with steel ball support particles and a coordination number of 4. If sand particles were used for the support, they were always of the same size and mineralogy as the particle being crushed. It was rare that significant damage occurred to the support particles. For the few occasions when it did happen, the tests were discarded.

The crushing mechanism was investigated for two types of sand. The first material was Leighton Buzzard sand (LBS), a quartz sand from the UK that has been extensively studied in the geotechnical field since the early 70s (Stroud, 1971). The second material was crushed limestone (LMS) from China made of weak and angular calcite particles. The crushed limestone is a diagenetic rock, consolidated (compressed) to large stress levels, and thus, unlikely to have significant intra-particle voids or internal defects as, for example, biogenic sands or weathered soils would show. Zhao et al. (2015) made CT scans of the LBS and highly decomposed granite (HDG) particles to relate the initial microstructure to the fracture mechanism. The LBS particles showed very few internal voids which did not influence the fracture pattern or the particles crushed with conchoidal fractures, as is expected with quartz. In contrast, the complex initial microstructure of the HDG particles, with intra-particle fissures, phase boundaries between different minerals, and cleavage in some of the minerals, meant that the fracture patterns were dominated by the internal particle structure with the coexistence of bending, shear, and tensile cracks along different features. Wang and Coop (2016) also used decomposed granite and LBS in their single particle tests. However, the complexity of the internal structure of the decomposed granite revealed by Zhao et al. meant that it was less suitable for the current study aimed at investigating the influence of the nature and the number of contacts on breakage. This is why crushed limestone was chosen instead as the second softer and weaker material.

The three descriptor diameters were defined for the particles in their at-rest position as the maximum and intermediate Feret diameters in the horizontal plane and the minimum in the vertical plane, measuring each with a Vernier calliper with a resolution of 0.01 mm. The use of a Vernier calliper was preferred to a digital image method for the measurements of the particle dimensions because it allowed for the characterisation of the large number of specimens required for the statistical analysis in a relatively short time, but did not jeopardise the measurement accuracy. The average minimum diameter, i.e., the thickness of the particle, was around 2.20 mm for both sands. The descriptor diameters, along with the shape characteristics and the

Table 1
Characteristics of the LBS and LMS particles (dimensions in mm, microhardness, HM, in GPa).

Material	d_{max}	d_{int}	d_{min}	S	r_{rl}	HM
LBS	3.61	2.90	2.21	0.63	0.48	6.2
LBS	2.62	2.15	1.62	–	–	6.2
LMS	3.46	2.70	2.24	0.69	–	1.6
LMS	2.41	1.86	1.51	–	–	1.6

global hardness of the materials, are indicated in Table 1. The shape descriptors were evaluated as sphericity S and roundness. In this study, however, it was preferred that a local roundness parameter be used in terms of the geometry of the grains at the contacts rather than the global roundness of the grains. The sphericity, S, was calculated from the two vertical side views as the ratio between the radii of the maximum inscribed and the minimum circumscribed circles defined from the outline of the particle (Krumbein and Sloss, 1963). The side views were obtained from high-quality images in two orthogonal directions. The formula, which accounts for the average sphericity from both side views, is given in Eq. (1).

$$S = \sqrt{S_A S_B} = \sqrt{\frac{r_{max,Inc.,A}}{r_{min,circ,A}} \cdot \frac{r_{max,Inc.,B}}{r_{min,circ,B}}} \quad (1)$$

where A and B refer to the different side views, S is the sphericity, $r_{max,inc}$ is the maximum inscribed radius, and $r_{min,circ}$ is the minimum circumscribed radius.

A new parameter, the relative local roundness, r_{rl}, was defined to quantify the local outlines of two particles at their contacts. An image-processing technique was used both in the quantification of this and the sphericity. Pictures of the particles were first transformed into a binary format and then, for r_{rl}, a polynomial function f(x) of the fifth order was used to fit the outline of the binary image using Matlab. The fifth order function was the best fit of the particle outlines. Fig. 3 shows a comparison between a typical particle outline and the fitting quality of the polynomial functions of different orders. At the high magnification shown here, the pixel size of the captured image is evident, but it is clear that functions of lower degrees are too inaccurate to characterise the local curvature, while the sixth order did not show better accuracy. The whole particle perimeter was divided into two parts so that the digitised outline was only a function of one independent variable (x). The radius of curvature $r_i(x)$ of one contact point was calculated according to the general formula for the curvature, χ, of a given function, f(x), as follows:

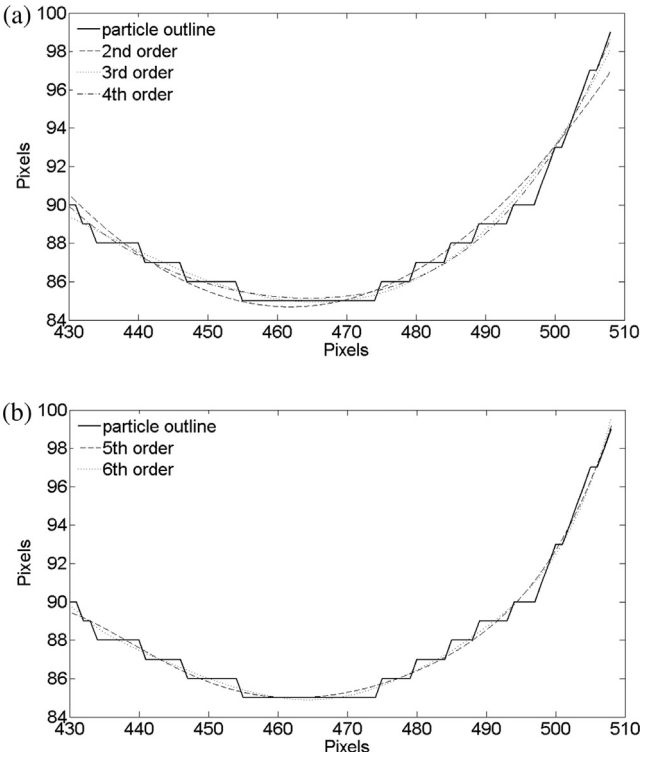

Fig. 3. Fitting of particle outline by polynomial functions of different orders: (a) 2nd, 3rd and 4th orders and (b) 5th and 6th orders.

$$\chi = \frac{1}{r_i(x)} = \frac{|f(x)''|}{(1 + (f(x)')^2)^{3/2}} \quad (2)$$

where f(x) is the function at the point (x) selected on the contact surfaces. The radius of curvature of each particle r_j was calculated as the average of $r_i(x)$ along the whole contact region:

$$r_j = \sum_{i=1}^{N} \frac{r_i(x)}{N} \quad (3)$$

where N is the number of points that defined the function f (x) along the contact region. Since the test configuration meant that the crushed particle was in contact with others, a measure of the geometry for each contact was established as follows (Eq. (4)):

$$r_{1,j} = \frac{r_1 r_j}{r_1 + r_j} \quad (4)$$

where 1 refers to the crushed particle and j to the j-th particle which was in contact with particle 1. The r_{rl} was then defined as the minimum $r_{1,j}$ divided by the thickness of the crushed particle, $d_{1,min}$, in order to create a parameter independent of the particle size (Eq. (5)). The procedure for the calculation of the shape descriptors is shown in detail in Fig. 4, where the functions f(x) are schematised as arcs and only three views are presented for simplicity (arcs were not used in the actual calculations).

$$r_{rl} = \frac{\min(r_{1,j})}{d_{1,min}} \quad (5)$$

The calculation of r_{rl} may be conducted in 2-D or 3-D. In 3-D, the contacts were not only assessed from the front view, but different orientations were considered in order to give optimum and complete views of the contacts. For example, five pictures were generally taken for each CN4 configuration (three at the bottom and two at the top). Wang and Coop (2016) conducted only single-particle crushing tests, but demonstrated that there was no significant difference between using a 2-D or 3-D parameter. Ideally the contact geometry could be quantified most accurately using CT scanning, (e.g., Fonseca et al., 2013), but it would be impractical to scan a sufficient number of tests to be able to establish the characteristic stress: survival probability curves.

The high-speed camera was used to record the crushing process during the tests. The videos were post-processed in

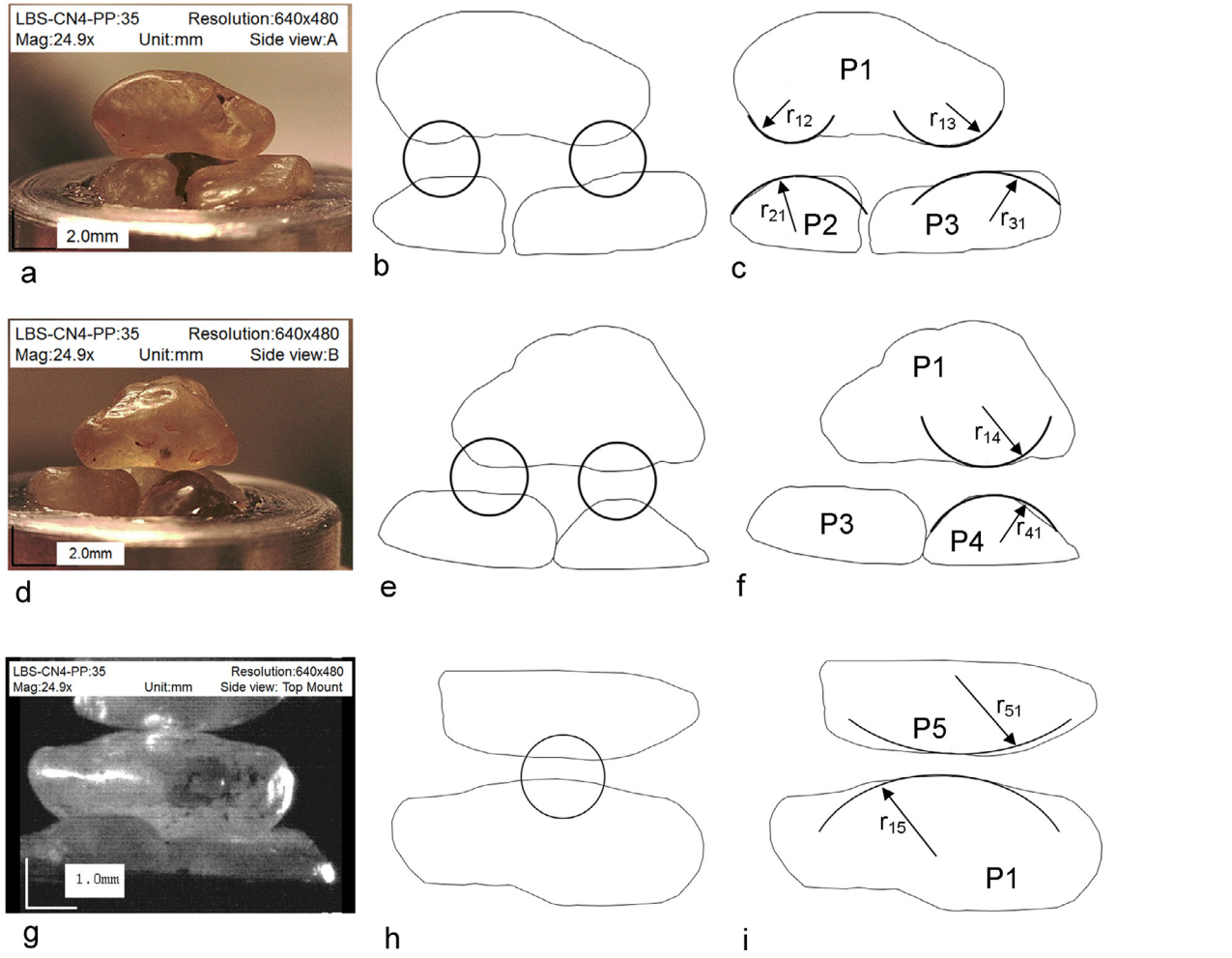

Fig. 4. Example of local relative roundness parameter, r_{rl}, of test No. 35, LBS-CN4-PP based on 3 views: (a) side view A of lower mount; (b) location of contact points of side view A; (c) definition of local radius of curvature for each contact of side view A; (d) side view B of lower mount; (e) location of contact points of side view B; (f) definition of local radius of curvature for each contact of side view B; (g) view of top mount; (h) location of contact points at top mount; and (i) definition of local radius for contact at top. The arrows are indicative.

order to locate the initiation of the failure crack within the particle and to characterise the crushing mechanism. The Weibull criterion was applied to the data analysis and the failure stresses were obtained from Eq. (6), which assumes a tensile failure:

$$\sigma_f = \frac{F}{\pi\left(\frac{d_{int}}{2}\right)\left(\frac{d_{min}}{2}\right)} \tag{6}$$

where F is the maximum force recorded from the test, and d_{int} and d_{min} are the intermediate and minimum diameters of the crushed particle, respectively. Considering the failure area of the particle as the geometric mean of the d_{int} and d_{min} diameters allows for consideration of the effect of the particle morphology, especially in the case of elongated particles. An example of the effect of the failure area on the particle strength is shown in Fig. 5 where three different survival probabilities, obtained from the geometric mean area (present study), the circle area (Nakata et al., 1999), and the circle area increased by a factor of 1.1, as adopted

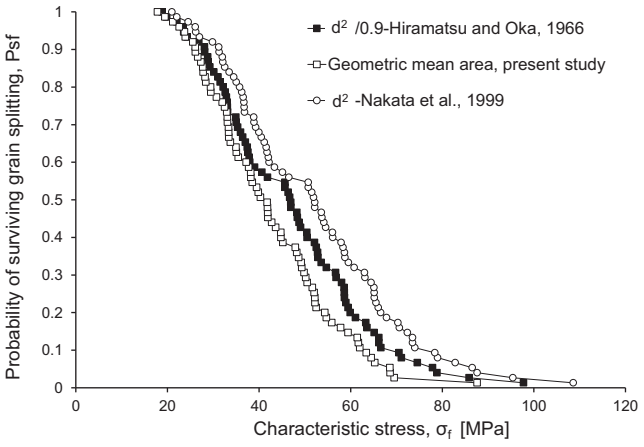

Fig. 5. The effect of the failure area on the strength of the LBS particles crushed between two hardened steel mounts, i.e., LBS-SP. The geometric mean area has been adopted in this study.

by Hiramatsu and Oka (1966), are compared. The use of Eq. (6) implies a simplistic stress regime within the particles at failure that is undoubtedly far from reality, particularly for the CN4 and CN6 tests. However, it is probably preferable, as a means of comparison, to using the failure forces, although the conclusions would be the same whether the analysis was in terms of force or stress. The calculation of the characteristic stress is based on the total force acting on the system, which must all be transmitted through the central crushed particle, although of course the local contact forces will be lower for a higher CN.

Todisco et al. (2015) observed different contact behaviours between quartz and calcite grains and underlined that the hardness of particles at the contacts was an important factor in characterising the crushing mechanism. However, they based their relationship on generic mineral hardness values available in the literature. The micro-hardness values of LBS and LMS grains have now been measured in order to describe the contact properties in a more accurate way. A Fisherscope HM2000XYp was used on fresh particle surfaces with an indentation force of 1 N for both materials. Both the polishing and the grinding of the particle surfaces were avoided since these actions may affect the residual stress state, and thus, the hardness (Griepentrog et al., 2002). The micro-hardness values reported in Table 1 refer to Martens hardness (HM) which is the ratio between maximum specified force F and surface area A(h) of the Vickers indenter penetrating from the zero point of the contact:

$$HM = \frac{F}{A(h)} = \frac{F}{h^2 \frac{4\sin\left(\frac{\alpha}{2}\right)}{\cos^2\left(\frac{\alpha}{2}\right)}} \quad (7)$$

where α is the angle between the two opposite faces of the Vickers indenter and h is the depth of the indentation. Several specimens of LBS and LMS were glued onto a steel mount with resin epoxy, and the flattest surfaces of each were indented at three different locations by means of a microscope. The average value of HM for the LBS grains was 6.2 GPa and that of LMS was 1.6 GPa.

3. Results

Weibull statistics are presented for both the LMS and LBS particles along with the m-moduli, but the effect of the geometry of the contacts on the crushing mechanism is examined only for the LBS particles. It was not possible to calculate the local relative roundness of the LMS particles due to the geometry of the contacts, which often consisted of flat-to-flat surfaces (Fig. 6). In contrast, accurate values of r_{rl} could be calculated from the geometry of the contacts of the LBS particles. The total number of tests and the number of them used for the study of morphology are indicated in Table 2. Within the study of the effects of morphology, those tests that showed incipient cracks at the top of the crushed particle and also the number of tests that have not been considered in a more detailed analysis of morphology are highlighted.

Fig. 6. Flat-to-flat contacts between LMS particles.

3.1. Effects of particle morphology and hardness

In order to take into account the particle sphericity, the tests on the LMS particles were divided into two groups. The first group was used to determine the probability of survival of particles characterised by values of sphericity ranging between 0.5 and 0.7, while the second probability curve was generated for the more spherical particles. Similar trends could be identified for both the CN4-PP and CN6-PP tests as presented in Fig. 7, where the more spherical particles appear to be generally weaker. However, for very weak particles (σ_f less than 10 MPa) the trend is reversed. Unland and Al-Khasawneh (2009) investigated the influence of the shape of limestone particles in impact crushing tests and found that fewer spherical particles were stronger.

The same selection was applied to the LBS specimens, for which the sphericity ranges chosen were between 0.4–0.6 or 0.6–0.8 for the CN4 tests and 0.5–0.7 or 0.7–0.9 for the CN6 tests. In contrast to the LMS behaviour, the data for the LBS particles show that the sphericity has no clear effect on the failure stress, as shown in Fig. 8. For the LBS, the effect of the relative local roundness at the contacts, r_{rl}, was evaluated by dividing the data into three groups of $r_{rl} = 0.2$–0.4, 0.4–0.5, and 0.5–0.7. The results show that particles with lower r_{rl}, i.e., sharper contacts, are weaker than particles showing more rounded contact geometries (Fig. 9).

It might be inferred that for stronger particles, like the LBS, the geometry of the contacts dominates the crushing mechanism, obscuring the effect of the overall particle shape. When the contacts are sharp, i.e., lower r_{rl}, the particle experiences large stress concentrations at the contacts which may lead to crack initiation in the proximity of the sharp contact before the stresses can redistribute inside the whole particle. On the contrary, soft particles do not experience any stress concentration at the contacts because

Table 2
Description of the tests.

Test configuration	Number of tests			
	Total	Study of morphology		
		Tests for morphology	Initiation of the crack at the top of the particle	Not considered (no video available)
LBS-SP	90	76	8	–
LBS-CN4-BP	59	–	–	–
LBS-CN6-BP	34	–	–	–
LBS-CN4-PP	70	65	6	8
LBS-CN6-PP	65	51	–	–
LBS-CN6-PPsmall	44	30	–	–
LMS -SP	28	24	–	–
LMS-CN4-BP	39	–	–	–
LMS-CN6-BP	36	22	–	–
LMS-CN4-PP	56	51	–	–
LMS-CN6-PP	58	53	–	–
LMS-CN6-BPsmall	16	–	–	–

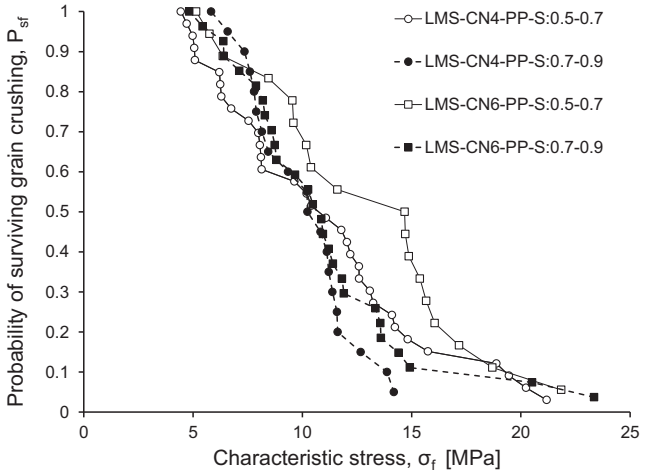

Fig. 7. Effect of sphericity on strength of LMS particles.

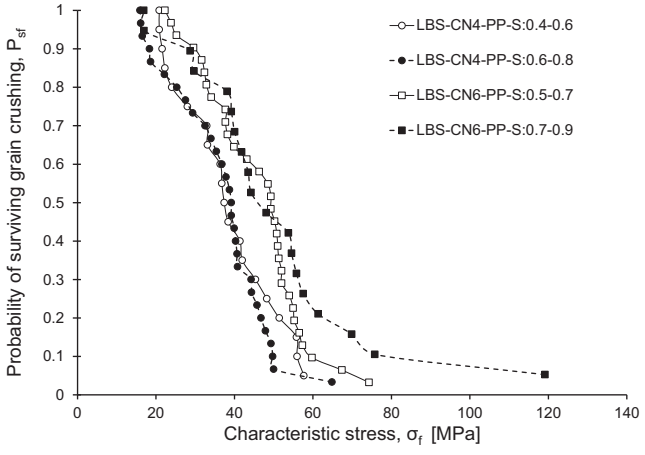

Fig. 8. Effect of sphericity on strength of LBS particles.

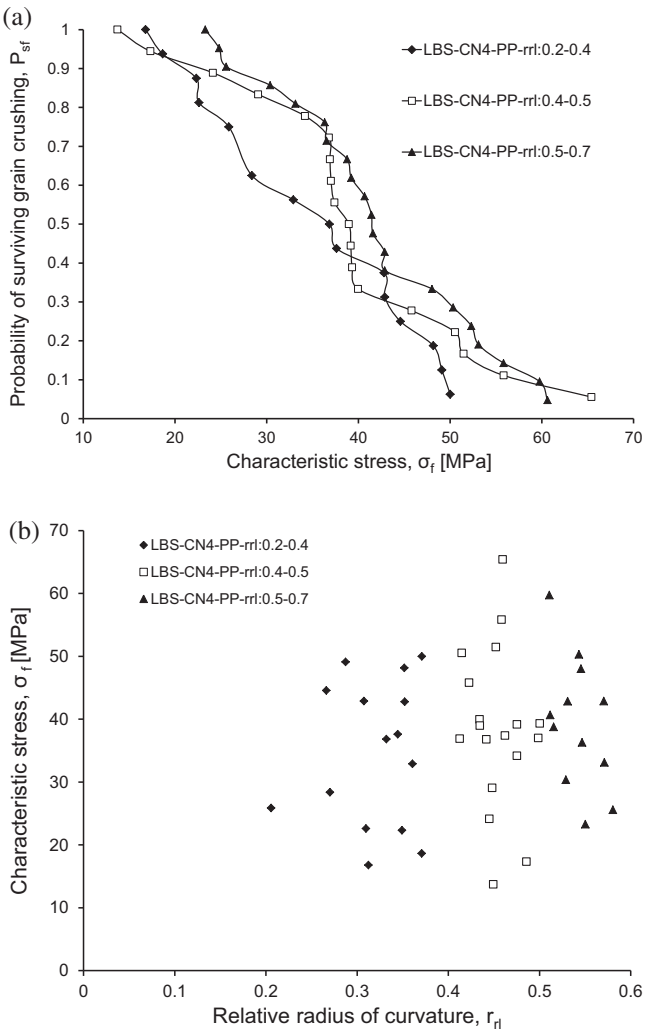

Fig. 9. Effect of local roundness parameter, r_{rl}, on LBS particles: (a) probability of surviving grain crushing and (b) relationship between characteristic stress and r_{rl}.

they mould relative to the neighbouring particles, and so, the whole particle participates in the crushing process. An example of this inference is shown for the LMS in Fig. 10 where, as loading proceeds, the displacements are large, but there is no initial evidence of overall failure. Instead, it seems that the contacts deform substantially, to the point where the central particle starts to be obscured. This phenomenon must be associated more with the hard-

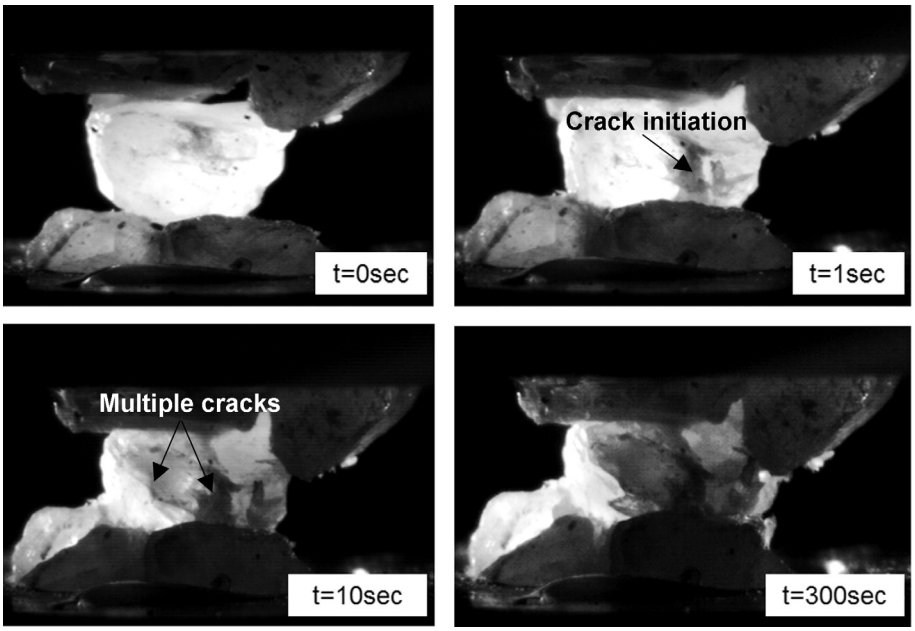

Fig. 10. Example of crushing mechanism of LMS particles tested in CN6-PP configuration.

ness of the limestone than with its stiffness since the Young's modulus of calcite is 73–84 GPa, while that of quartz is only slightly higher at 94–98 GPa (Mavko et al., 1998; Jaeger et al., 2007).

The influence of sphericity on the crushing of the LMS particles contradicts the work of Hiramatsu and Oka (1966) who found, both by means of photo-elasticity and experiments, that the stress field inside an irregular piece of rock may be considered the same as that within a sphere, and that the tensile stress in the rock, subjected to a pair of opposing forces, agrees well with that calculated for a sphere if the latter is reduced by a factor of 0.9.

In Fig. 11, the failure stress of LMS is related to that of LBS for the test configurations of CN6-PP and CN4-PP. Each data point represents the failure stress selected at the same survival probability value on the curves of LMS and LBS, respectively, so that lower values of stress describe higher probabilities of survival. The gradient of this relationship is 0.30, which is similar to the ratio of the micro-hardness values of the LBS and LMS particles. This result suggests that the micro-hardness may play a significant role through the deformation of the contacts.

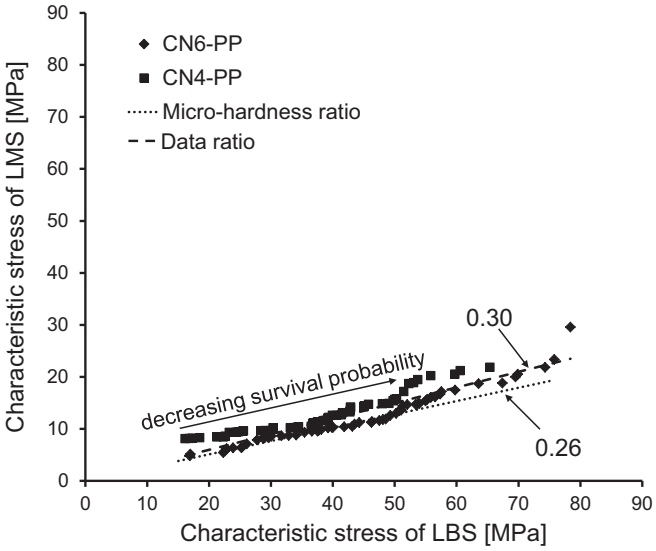

Fig. 11. Hardness relationship obtained from characteristic stress of LBS and LMS specimens crushed in CN4-PP and CN6-PP configurations.

3.2. Effect of support particles

In Fig. 12, the survival probability curves for the CN6 configuration for the LBS clearly show that the particles crushed between steel balls are stronger than those crushed between particles, but that no significant difference can be observed between the two types for the CN4 configuration. On the other hand, the LMS particles give similar survival probabilities for all the test configurations, as presented in Fig. 13. Indeed, the maximum variation between the characteristic stresses at a survival probability of 37% for LMS particles crushed in SP, CN4-BP, and CN6-BP configurations was only 1 MPa. A small number of tests were also carried out on smaller particles which show larger failure stresses than the larger particles, as expected (Nakata et al., 1999).

This dissimilarity may be attributed to the different natures of the contacts which are established between strong and soft particles. The geometry of the contacts of a quartz particle is preserved during the test, and large stress concentrations might occur at the contacts as they transfer the load without changing their morphology significantly. When a quartz grain is compressed between 6 steel balls, each contact experiences less stress concentration than

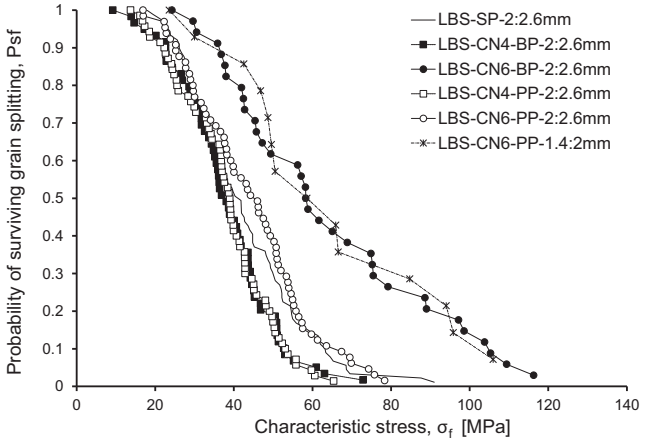

Fig. 12. Survival probability curves of LBS particles for different support particles.

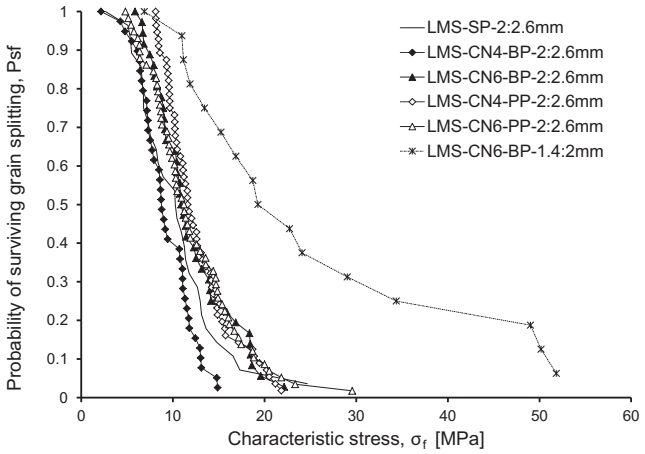

Fig. 13. Survival probability curves of LMS for different support particles.

during loading of between 4 and 2 points. On the other hand, the geometry of the soft contacts of an LMS grain is not preserved during loading or moulding relative to the neighbouring contacts; hence, the stress distribution may vary much less when the LMS grain is crushed between hard (steel balls) or soft (LMS particles) materials.

3.3. Effect of coordination number

The force-displacement curves of uniaxial compression tests (SP) and particle to particle tests (CN4 and CN6) for LBS and LMS are presented in Fig. 14 (the data for LMS are redrawn from Todisco et al., 2015). Test LBS-CN6-PP shows stick-slip behaviour due to some small movement at the particle contacts. Generally, the increase in the coordination number did not change the crushing behaviour of the quartz or the limestone particles, as seen in these figures, or the failure mechanisms. The LBS particles showed brittle failure (the curves are monotonic and the displacements are small) with the development of conchoidal fractures, whereas the LMS particles failed in a

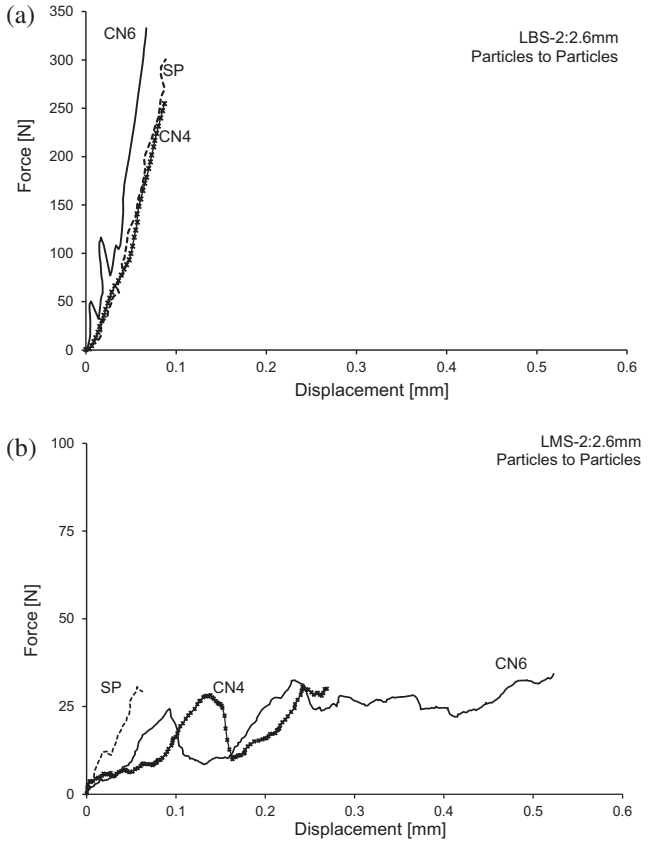

Fig. 14. Force-displacement relationship of (a) LBS (present study) and (b) LMS (redrawn from Todisco et al., 2015) particles.

ductile way reaching larger displacements and showing a saw-tooth shaped curve. It might be expected that the failure force should increase with the increase in the coordination number, and Fig. 14 already shows an example of this variation. For the LBS grains, the CN6 configuration leads to a larger failure force than CN4 or SP which are quite similar. This suggests that the location of the applied loads does not influence the particle strength for SP or CN4. The effect of the coordination number on the failure force of the LMS particles in Fig. 14 is less pronounced due to the soft nature of the contacts.

In Fig. 12, the effect of the coordination number is quite clear for the quartz particles which are more prone to break when subjected to diametrically opposite forces (SP) than those subjected to a more complex system of forces (CN6). At the 37% probability, the characteristic stress of particles crushed between two steel platens is generally lower (45 MPa) than that calculated for the particles crushed between other particles. For example, the characteristic stress of LBS-CN6-PP is 51 MPa and that of LBS-CN6-BP is 71 MPa. The CN4 configuration does not have a clear effect on the particle strength. This might be attributed to the configuration of the loading points, where there are three contact points at the base and one at the top, which may resemble more that of a single-particle crushing test since in this configuration the particle

will always rest on three points at its base prior to the loading process. Therefore, it might be difficult to see a net variation between the strength obtained from the SP and CN4 tests.

For the LMS particles, as explained in Section 3.2, the effect of the coordination number is less clear, as shown in Fig. 13, although the characteristic stresses for the CN6-PP tests are still slightly higher than for the other test configurations. Configuration CN4-BP overlaps that of the single-particle crushing test (SP) for probabilities larger than 60%. This underlines that the location of the applied loads does not influence the particle strength for soft particles either. The factor that accounts for the variability of strength within the population of particles is the m-modulus, which is used to describe the uniformity of the strength σ of a population of grains and increases with a decrease in the variability of the particle strength. It generally varied from 2 to 5 for LMS and from 3.5 to 4.5 for LBS (Fig. 15), but no influence of the test configuration could be found for the m-modulus.

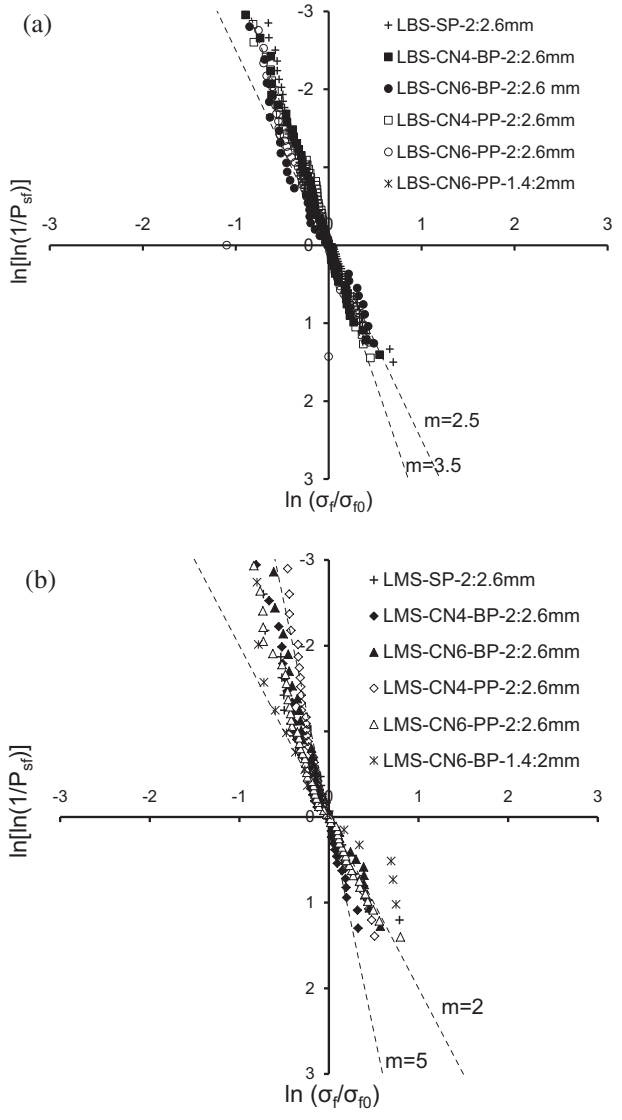

Fig. 15. The m-modulus of tested sands: (a) LBS specimens and (b) LMS specimens.

Simplified failure criteria developing for a disc can be used to explain why a particle subjected to diametrical forces is more prone to break than one subjected to a set of forces. Detailed explanations are given in the failure models of Tsoungui et al. (1999) and Ben-Nun and Einav (2010). When a grain is subjected to a complex state of stress, its stress condition can be reduced to the state of principal stresses in the first order, which compress the particle by hydrostatic pressure p and deviatoric stress τ. When the tensile stress becomes greater than the threshold stress, a crack initiates at the disc centre and the grain fails by tensile splitting. The expression given in Eq. (8) (Tsoungui et al., 1999) implies that a grain has a higher probability of splitting when the deviatoric stress, 2τ, is much larger than the hydrostatic pressure, p, i.e., when diametrical forces act on the particle:

$$\sigma_{xx}^{0} = 2\tau - p \geqslant \sigma_{crit}(R) \tag{8}$$

where σ_{xx}^{0} is the tensile stress acting at the disc centre, and $\sigma_{crit}(R)$ depends on the nature of the material, the dimensions of the grain, and the Weibull modulus, m.

Another example of a failure criterion which considers the role of the coordination number is that of Ben-Nun and Einav (2010). In their failure model of a grain subjected to isotropic loading from neighbouring grains, they considered the possibility that the crack initiates through in-plane shear fractures, i.e., mode II of Irwin's (1957) failure criteria. In this case, the authors proposed a threshold of F_{crit} equal to

$$F_{crit} = d\sigma_{crit} f_w f_d f_{CN} \tag{9}$$

where d is the thickness of the grain, σ_{crit} is the tensile stress at failure for the largest particle, f_w is a factor accounting for particle imperfections, f_d is a factor considering the

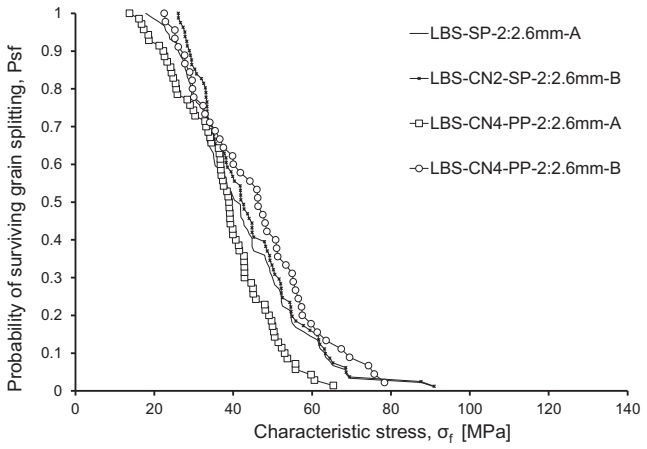

Fig. 16. Probabilities of survival of LBS particles for which crack initiation did not occur near top contact. Data refer to SP and CN4-PP configurations. (A all data and B with failures near top contact eliminated.)

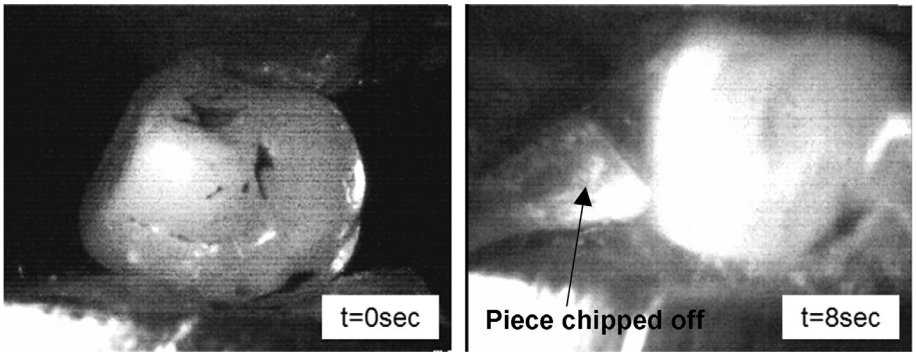

Fig. 17. Chipping crushing mechanism of LBS particle tested between 4 particles.

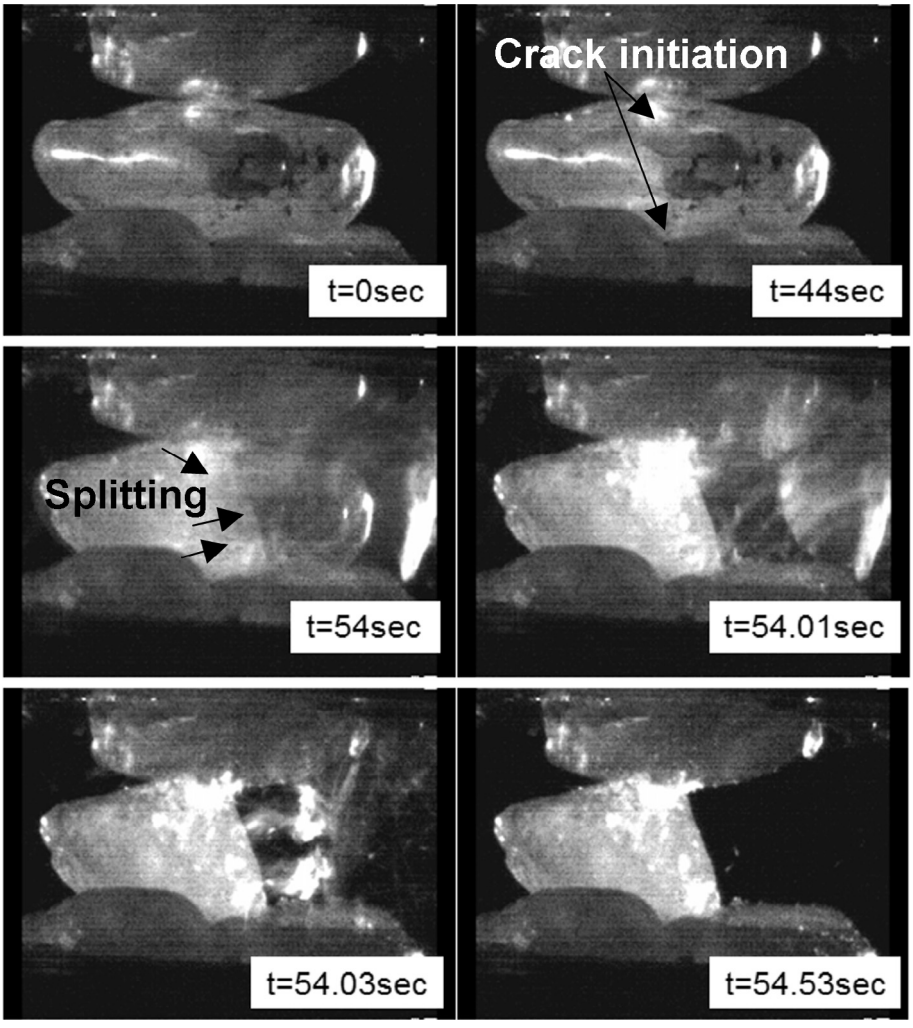

Fig. 18. Splitting crushing mechanism of LBS particle tested in CN4-PP configuration.

geometry of the particle at the contacts, and f_{CN} is a factor accounting for the effect of the coordination number on the crushing mechanism. The expression for f_{CN}, as given by Ben-Nun and Einav (2010) and shown in Eq. (10), implies that as the coordination number increases, the factor increases leading to an increase in the critical stress threshold:

$$f_{CN} = (CN - 1)e^{(D/d)(CN-2)(CN-3)/4CN} \quad (10)$$

where D is the diameter of the neighbouring particles, d is the dimension of the crushed particle, and CN is the coordination number of the crushed particle. From Eq. (9), an increase in F_{crit} is reflected as a decrease in the probability of failure of a grain with a higher coordination number.

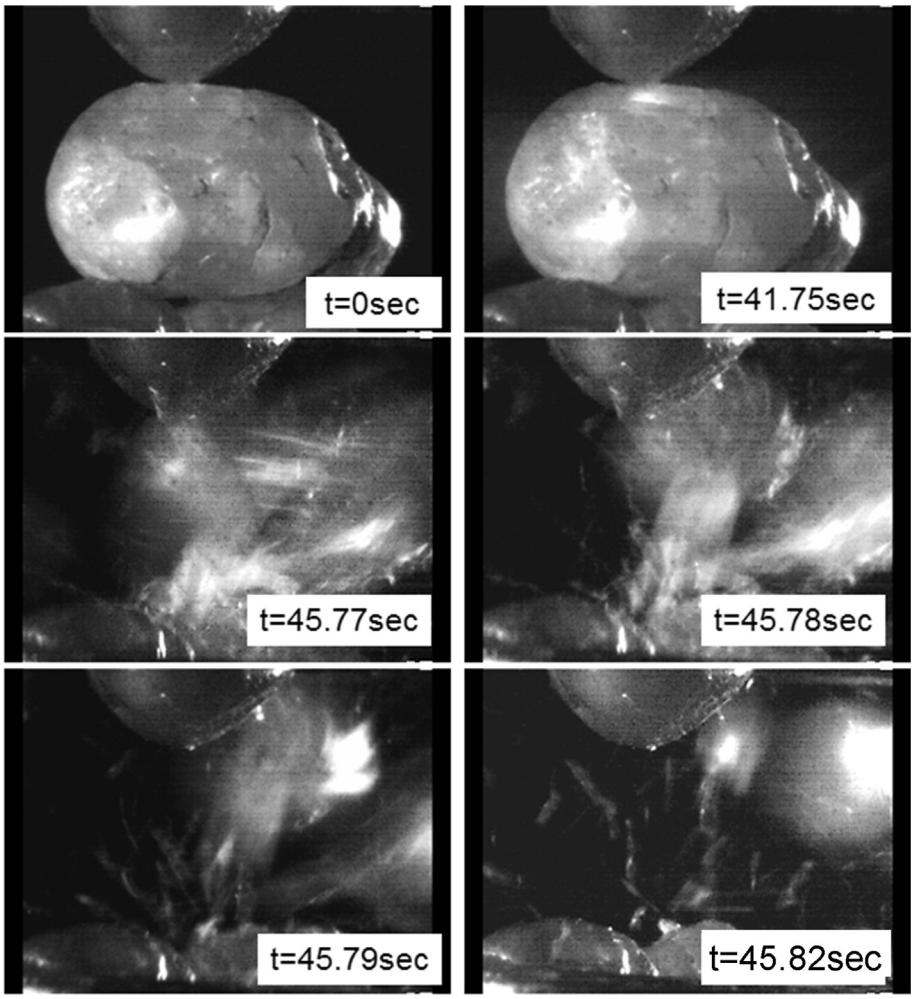

Fig. 19. Fragmentation crushing mechanism of LBS particle crushed between 4 particles.

3.4. Characterization of crushing mechanism

The characteristic stresses calculated here assume that the crushed particle failed in a tensile mode, obeying Griffith's criterion, for which a crack initiates in the centre of a disc when it is subjected to diametrical loads. Complete stress solutions for a grain that fails in tension under two opposite loads, acting on a finite arc, have been formulated by several researchers, Hondros (1959) and Hiramatsu and Oka (1966) among others, and they are used to calculate the tensile strength of a disc of rock in the Brazilian test (Eq. (11)).

$$\sigma = \frac{F}{\pi R t} \tag{11}$$

where the failure force (F) acts on the disc over an arc not greater than 10° (Li and Wong, 2013), and R and t are the radius and the thickness of the disc, respectively.

It has been argued that this formula might not be suitable for the estimation of the tensile strength of rock because the crack does not initiate in the centre, but near the loading point (Fairhurst, 1964; Li and Wong, 2013). Recently, Russell and Muir Wood (2009) formulated a model for a point-loaded sphere in which the crack initiation occurs when the ratio between the second invariant of the deviatoric stress tensor, J_2, and the first invariant of the stress tensor, I_1, is a maximum, which is essentially a maximum ratio of shear to normal stress invariants. In their work, the location of the initial failure was near the point load, at a distance between 0.7 and 0.9 from the centre of the sphere. In the present study, this possibility was considered by eliminating the tests which showed a failure at the top for CN4 and SP tests from the data, although they were small in number, as indicated in Table 2. The videos were recorded with the high-speed camera and the analysis was applied only to the LBS particles tested between steel platens (SP) or 4 other particles (CN4-PP). The CN6-PP configuration was not considered because, in this case, the crack initiation may occur anywhere within the particle, since the forces are more equally distributed around the grain. The LMS particles were not analysed because it was difficult to determine the initiation of the failure, because the large deformations at the contacts tended to obscure the central particle.

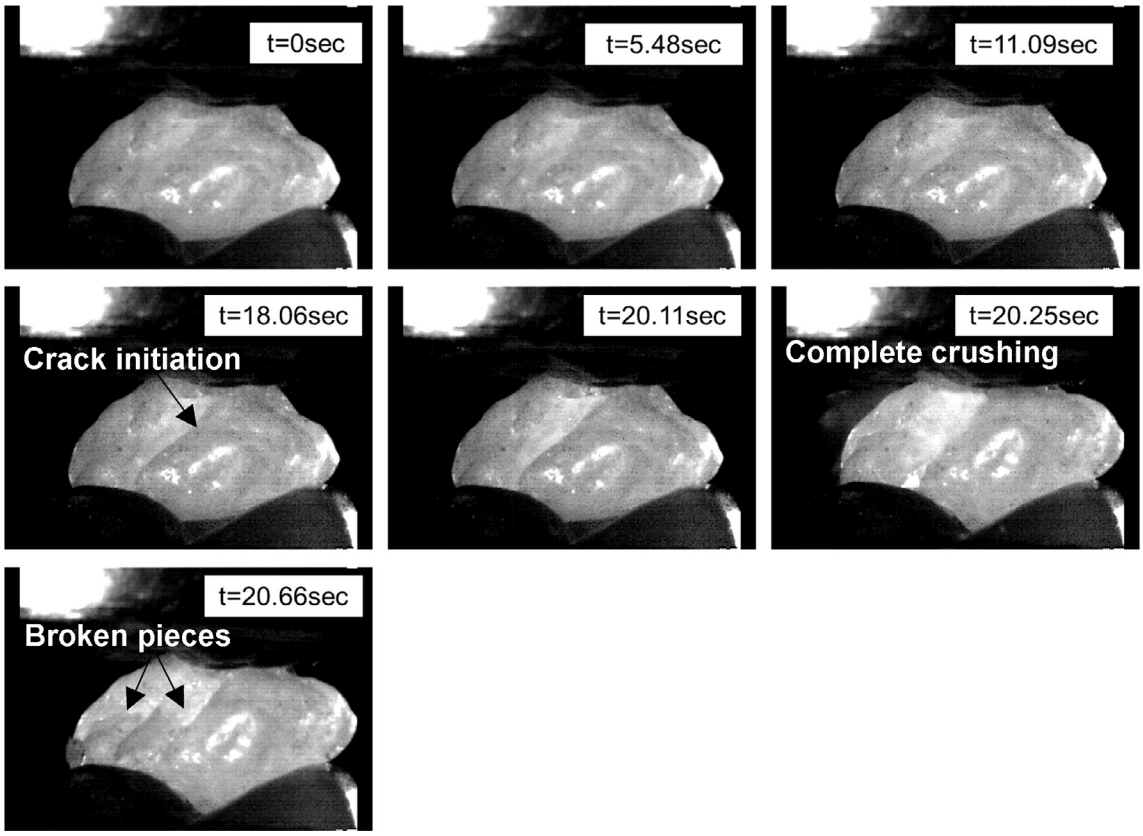

Fig. 20. Splitting crushing mechanism of LBS particle tested in CN6-PP configuration.

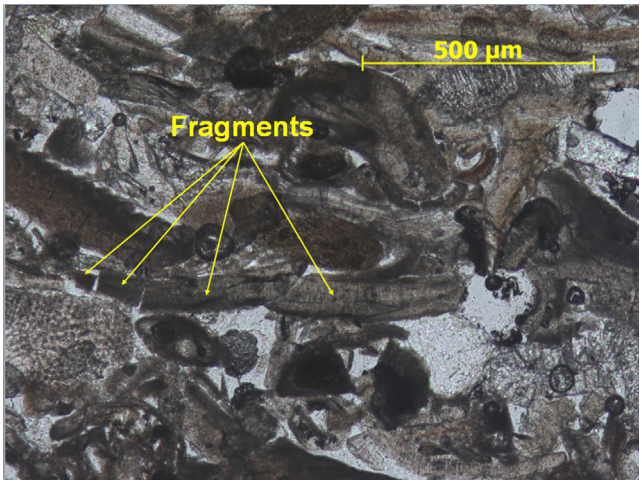

Fig. 21. Example of fragments of particle confined to their initial position (redrawn from Bandini and Coop, 2011).

As indicated in Table 2, only 8 out of 76 SP particles showed failure near the top contact. Failures near the base contact were not eliminated for the SP tests either, because the base contact should not be unique. Of the 14 CN4-PP tests discarded, 6 showed failure near the top contact and the remaining 8 were not taken into account because the location of the initial failure was unclear. The new probability curves shift to the right showing a small increase in particle strength (Fig. 16). This is more evident for the tests carried out in the CN4 configuration in which the characteristic stress increased from 45 MPa to 51 MPa, although a smaller number of tests was performed in comparison to the SP configuration. Any conclusion might be slightly speculative at this stage, because a large number of tests would be required to investigate whether this type of test is suitable for assessing the tensile strength of the sand particles in multi-axial loading tests.

The mode of failure was also analysed through the high-speed videos recorded during the tests. The two different sands behaved very differently, as expected. The soft LMS crushed into many pieces in a ductile way, reaching ultimate failure by the progressive breakage of the asperities and the large deformation of the contacts. Fig. 10 shows a sequence of the images captured during the video of the tests and this was seen to be typical of all the tests. The crushing mode of the quartz grains was analysed for both the CN4- and CN6-PP tests. The brittle failure, common for quartz, was divided into three categories: if a grain suddenly shattered into many tiny pieces, the crushing process was classified as fragmentation, while if the grain split into two or more large parts, the crushing process was classified as splitting. It was observed that some grains failed also due to the chipping of a smaller part of the particle not involving the entire particle in the crushing process, defined as "abrasion" by Tsoungui et al. (1999). Markides et al. (2010) found that discontinuities of stress and displacement fields concentrate at the edges of the load

contacts; and thus, the crack might initiate from the perimeter of the specimen. If it is made of hard material, this might not allow for a smooth transition of the crack from the edge through the less loaded part. Therefore, the failure occurs by the chipping off of a piece of the specimen and not by splitting or fragmentation.

The CN4-PP specimens involved all the three crushing categories. Out of the 32 tests for which a video was available, 25% failed due to fragmentation, 69% due to splitting, and 6% due chipping (Figs. 17–19). The particles of CN6-PP failed predominantly due to splitting, maintaining the two or three pieces generated from the crushing in place. An example is given in Fig. 20. The confinement given by this test configuration might cause this phenomenon. This brings to memory the behaviour of sand grains in triaxial tests, as observed by Bandini and Coop (2011), or oedometer tests by Bolton and Cheng (2002), in which a particle that breaks while it is surrounded by others tends to create fragments that are held in close proximity to each other after failure occurs, as shown Fig. 21.

4. Conclusions

Many factors may be involved in the complex mechanisms of the breakage of a sand grain. An analysis of the particle morphology and mineralogy, the nature, the geometry, and the number of contacts was conducted through multi-contact compression tests on sand particles. It was found that the sphericity affects the strength for soft materials, but not for hard materials, for which it seems to be obscured by the relative local roundness at the contacts. The more spherical the limestone particles were, the stronger they were, and sharper contacts led to a decrease in the failure stress for quartz particles. Material hardness is seen to be of key importance in the crushing mechanism; it may affect the particle strength through the deformation of the contacts. The main difference between the crushing behaviour of quartz and calcite grains was therefore attributed to the nature of the contacts. Hard contacts preserve their morphology during loading, experiencing large stress concentrations prior to failure. Soft contacts mould relative to their neighbouring particles, involving the entire particle in the crushing mechanism.

Generally, an increase in the number of contacts induced an increase in particle stress at failure. The assumption of a tensile failure was adopted to determine the Weibull probability of the populations of sand particles, but a much larger number of tests would be needed to assess whether or not this approach is suitable for calculating the tensile strength of sand particles, which would be highly time-consuming for these multiple contact tests.

If the coordination number was four, either in the CN = 4 or SP tests, then failure occurred by splitting, fragmenting or chipping, but in the CN = 6 tests, generally only splitting occurred, maintaining the products of the crushing in place.

Acknowledgements

The work described in this paper was fully supported by a grant from the Research Grants Council of the Hong Kong Special Administrative Region, China (Project No. CityU 112712).

References

Altuhafi, F.N., Coop, M.R., 2011. Changes to particle characteristics associated with the compression of sands. Géotechnique 61 (6), 459–471.

Bandini, V., Coop, M.R., 2011. The influence of particle breakage on the location of the critical state line of sands. Soils Found. 51 (4), 591–600.

Ben-Nun, O., Einav, I., 2010. The role of self-organization during confined comminution of granular materials. Philos. Trans. R. Soc. A 368, 231–247.

Bolton, M.D., Cheng, Y.P., 2002. Micro-geomechanics. In: Lisse, Springman (Eds.), pp. 59–69.

Coop, M.R., Sorensen, K.K., Bodas Freitas, T., Georgoutsos, G., 2004. Particle breakage during shearing of a carbonate sand. Géotechnique 54 (3), 157–163.

Dean, W.R., Sneddon, A.M., Parsons, H.V., 1952. Distribution of Stress in a Decelerating Elastic Sphere. Selected Government Research Reports: Strength and Testing of Materials: Part II: Testing Methods and Tests Results. HSMO, London, pp. 212–234.

Drescher, A., De Jong, G. De Josselin, 1972. Photoelasticity verification of a mechanical model for the flow of a granular material. J. Mech. Phys. Solids 20 (5), 337–351.

Durelli, A.J., Wu, D., 1984. Loads between disks in a system of discrete elements. Exp. Mech. 24 (4), 337–341.

Fairhurst, C., 1964. On the validity of the Brazilian test for brittle materials. Int. J. Rock Mech. Min. 1, 515–526.

Fonseca, J., Nadimi, S., Reyes-Aldasoro, C.C., O'Sullivan, C., Coop, M. R., 2016. Image-based investigation into the primary fabric of stress-transmitting particles in sand. Soils Found. 56 (5), 818–834.

Fonseca, J., O'Sullivan, C., Coop, M.R., Lee, P.D., 2013. Quantifying the evolution of soil fabric during shearing using directional parameters. Géotechnique 63 (6), 487–499.

Griepentrog, M., Ullner, C., Duck, A., 2002. Instrumented indentation test for hardness and materials parameter from millinewtons to kilonewtons. In: 11th IMEKO TC05 Conference on Hardness Measurement, Celle, Germany, 24–26 September, pp. 53–58.

Gundepudi, M.K., Sankar, B.V., Mecholsky, J.J., Clupper, D.C., 1997. Stress analysis of brittle spheres under multiaxial loading. Powder Technol. 94 (2), 153–161.

Hiramatsu, Y., Oka, Y., 1966. Determination of tensile strength of rock by compression test of an irregular test piece. Int. J. Rock. Mech. Min. 3, 89–99.

Hondros, G., 1959. The evaluation of Poisson's ratio and the modulus of materials of a low tensile resistance by the Brazilian (indirect) test with particular reference to concrete. Aust. J. Appl. Sci. 10 (3), 243–268.

Irwin, G., 1957. Analysis of stresses and strains near the end of a crack traversing a plate. J. Appl. Mech. 24, 361–364.

Jaeger, J.C., Cook, N.G.W., Zimmerman, R., 2007. Fundamentals of Rock Mechanics, 4th ed. Wiley-Blackwell, Oxford.

Krumbein, W.C., Sloss, L.L., 1963. Stratigraphy and Sedimentation. W. H. Freeman and Company, San Francisco.

Li, D., Wong, L.N.Y., 2013. The Brazilian disc test for rock mechanics applications: review and new insights. Rock Mech. Rock. Eng. 46 (2), 269–287.

Markides, C.F., Pazis, D.N., Kourkoulis, S.K., 2010. Closed full-field solutions for stresses and displacements in the Brazilian disk under distributed radial load. Int. J. Rock Mech. Min. Sci. 47 (2), 227–237.

Mavko, G., Mukerji, T., Dvorkin, J., 1998. The Rock Physics Handbook: Tools for Seismic Analysis in Porous Media. Cambridge University Press, Cambridge.

McDowell, G.R., Bolton, M.D., 1998. On the micromechanics of crushable aggregates. Géotechnique 48 (5), 667–679.

McDowell, G., 2002. On the yielding and plastic compression of sand. Soils Found. 42 (1), 139–145.

Minh, N.H., Cheng, Y.P., 2013. A DEM investigation of the effect of particle-size distribution on one-dimensional compression. Géotechnique 63 (1), 44–53.

Muir Wood, D., 2008. Critical State and Soil Modelling. The Netherlands, IOS Press, Amsterdam, pp. 51–72.

Nakata, Y., Hyde, A.F.L., Hyodo, M., Murata, H., 1999. A probabilistic approach to sand particle crushing in the triaxial test. Géotechnique 49 (5), 567–583.

Russell, A.R., Muir Wood, D., 2009. Point load tests and strength measurements for brittle spheres. Int. J. Rock Mech. Min. Sci. 46 (2), 272–280.

Russell, A.R., Muir Wood, D., Kikumoto, M., 2009. Crushing of particles in idealised granular assemblies. J. Mech. Phys. Solids 57 (8), 1293–1313.

Stroud, M., 1971. Sands at Low Stress Levels in the S.S.A., s.l.: Cambridge University.

Tavares, L., 2007. Breakage of single particle: quasi-static. In: Handbook of Powder Technology, Vol. 12. Elsevier, s.l., pp. 3–68.

Todisco, M.C., Coop, M.R., Senetakis, K., Guo, Q., 2015. The effect of coordination number on particle crushing. Geomechanics from Macro to Micro, In: Proceedings of the TC 105 ISSMGE, IS-Cambridge 2015, vol. 2, pp. 1063–1068.

Tsoungui, O., Vallet, D., Charmet, J.C., 1999. Numerical model of crushing of grains inside two-dimensional granular materials. Powder Technol. 105 (1), 190–198.

Unland, G., Al-Khasawneh, Y., 2009. The influence of particle shape on parameters of impact crushing. Miner. Eng. 22 (3), 220–228.

Wang, W., Coop, M.R., 2016. An investigation of breakage behaviour of single sand particles using a high-speed microscope camera. Géotechnique. http://dx.doi.org/10.1680/jgeot.15.P.247.

Weibull, W., 1951. A statistical distribution function of wide applicability. J. Appl. Mech., 293–297

Zhao, B., Wang, J., Coop, M.R., Viggiani, G., Jiang, M., 2015. An investigation of single sand particle fracture using X-ray microtomography. Géotechnique 65 (8), 625–641.